Environmental Pollution 383 (2025) 126798

Contents lists available at ScienceDirect

Environmental Pollution

journal homepage: www.elsevier.com/locate/envpol

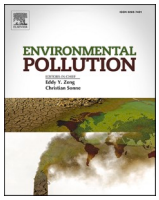

Dynamics of metal immobilization in coastal mariculture sediments: Insights from DGT and DIFS modeling☆

Yang-Guang Gu [a,e,f,*], Yanpeng Gao [b], Richard W. Jordan [c], Shi-Jun Jiang [d]

[a] South China Sea Fisheries Research Institute, Chinese Academy of Fishery Sciences, Guangzhou, 510300, China
[b] Institute of Environmental Health and Pollution Control, Guangdong University of Technology, Guangzhou, 510006, China
[c] Faculty of Science, Yamagata University, Yamagata, 990-8560, Japan
[d] State Key Laboratory of Marine Resource Utilization in South China Sea, Hainan University, Haikou, 570228, China
[e] Guangdong Provincial Key Laboratory of Fishery Ecology and Environment, 510300, Guangzhou, 510300, China
[f] Key Laboratory of Open-Sea Fishery Development, Ministry of Agriculture and Rural Affairs, Guangzhou, 510300, China

ARTICLE INFO

Keywords:
Metals
Diffusive gradients in thin films (DGT)
Kinetic modeling
Metal immobilization
Ecological risk
Zhelin Bay

ABSTRACT

Coastal sediments play a crucial role in regulating the mobility and bioavailability of metals in marine ecosystems, especially in aquaculture-dominated environments. This study conducted a dynamic assessment of metal release in the sediments of Zhelin Bay, the largest seawater aquaculture region in eastern Guangdong, China, using Diffusive Gradients in Thin Films (DGT) technology and the DGT Induced Fluxes in Sediments (DIFS) model. The distribution patterns of time-dependent R values for ten metals (Al, Cr, Mn, Fe, Co, Ni, Cu, Zn, Cd, and Pb) were analyzed alongside the adsorption (K_f) and desorption (K_b) parameters to elucidate the mechanisms by which metals are immobilized in sediments, limiting their release into the water column. Both the time-dependent R value patterns and K_f/K_b ratios demonstrated that all ten metals exhibited varying degrees of stabilization within the sediment, confirming their immobilization mechanisms in place. The maximum total concentration of Zn reached 347.82 mg/kg, corresponding to a moderate pollution level based on the geo-accumulation index. DGT-labile metals posed a joint ecological risk probability of 27.30 %, mainly due to Mn (11.19 %) and Al (11.15 %). These findings suggest that aquaculture activities and terrestrial nutrient inputs contribute to organic matter accumulation and biogeochemical shifts in sediments, influencing metal stabilization. This study is among the first to quantitatively characterize the dynamics of metal immobilization in coastal mariculture sediments using a combined DGT–DIFS approach.

1. Introduction

Coastal sediments serve as important regulators of metal cycling in marine environments, acting as both sinks and potential sources of pollutants (Jiskra et al., 2021; Gu et al., 2022a; Li et al., 2023a; Zitoun et al., 2024). The behavior of metals in these sediments is influenced by various factors such as organic matter content, biogeochemical cycles, and human activities (Gu et al., 2022a; Luo et al., 2022; Man et al., 2022; Kumar Chaudhary et al., 2023). In areas where marine aquaculture is prominent, such as the bays along the southern coast of China, intensive aquaculture practices—including fish cages, shellfish farming, and seaweed cultivation—have introduced substantial organic material and nutrients into the ecosystem, altering sediment properties and potentially affecting metal dynamics (Gu et al., 2014a; Gu et al., 2023a; Long et al., 2024; Wang et al., 2025).

In such aquaculture-dominated coastal environments, the interaction between sediments and metals is complex (Gu et al., 2014a; Miranda et al., 2021; Li et al., 2023a). Metal adsorption and desorption processes are critical in determining whether metals remain immobilized in the sediment or become bioavailable to aquatic organisms, thus posing potential ecological risks (Gu et al., 2022a; Li et al., 2023b). Metals can form stable complexes with organic matter or sulfides, limiting their release and bioavailability—a process sometimes referred to as metal immobilized (Falkowski et al., 2008; Gu et al., 2014a; Dong et al., 2023b; Sun et al., 2023). Understanding these dynamics in a typical marine aquaculture bay is crucial for developing management strategies aimed at minimizing ecological harm.

In recent years, increasing attention has been paid to the complex

☆ This paper has been recommended for acceptance by Maria Cristina Fossi.

* Corresponding author. South China Sea Fisheries Research Institute, Chinese Academy of Fishery Sciences, Guangzhou, 510300, China.
E-mail address: hydrobio@163.com (Y.-G. Gu).

https://doi.org/10.1016/j.envpol.2025.126798
Received 22 January 2025; Received in revised form 2 June 2025; Accepted 7 July 2025
Available online 8 July 2025

dynamics of metal remobilization and bioavailability in aquatic sediments under both equilibrium and non-equilibrium conditions. The diffusive gradients in thin-films (DGT) technique has emerged as a robust tool for elucidating the mobility, fluxes, and diagenetic behavior of trace metals and oxyanions in coastal sedimentary environments (Gao et al., 2022). Complementary methods—such as DGT-induced flux in sediments (DIFS) modeling, high-resolution dialysis, and stable isotope-labeled bioassays—have been employed to explore metal desorption kinetics, diffusion characteristics, and redox-mediated transformations at the sediment–water interface in freshwater and estuarine systems (Lin and Pan, 2023; Liu et al., 2023; Xu et al., 2024). However, these advancements have rarely been extended to marine aquaculture bays, which are particularly susceptible to anthropogenic pressures and organic matter enrichment from intensive mariculture. The dynamic behavior of metals in such environments—including their mobility, speciation, and short-term bioavailability during sediment disturbance—remains largely unexplored. While studies in reservoirs and estuaries have revealed complex flux patterns under varying hydrodynamic and redox conditions (Norgbey et al., 2021; Liu et al., 2023; Liu et al., 2023; Xu et al., 2024), their findings cannot be directly extrapolated to marine aquaculture settings. Moreover, although kinetic models such as the DIFS model show promise for simulating metal fluxes and availability, their application in these coastal systems is still limited.

This critical knowledge gap reveals the urgent need for integrated approaches that combine high-resolution in situ passive sampling (e.g., DGT), kinetic modeling, and ecological risk assessment. Addressing this issue is essential for understanding and predicting metal behavior in aquaculture-impacted marine sediments, and for informing sustainable management of these vulnerable coastal ecosystems under intensifying human influence.

China is the largest producer and exporter of aquatic products, with its fishery production accounting for 74.9 % of the world's aquaculture output (Gu et al., 2023b; Li et al., 2023a). Given this dominant position, China plays a central role in shaping the direction of global aquaculture development. Guangdong Province, as China's top producer of aquaculture products, is particularly significant for understanding the broader environmental impacts of marine farming on coastal ecosystems (PRC State Council, 2024; Ray et al., 2025). Zhelin Bay, located in eastern Guangdong Province, is the largest seawater aquaculture bay in the region (Gu et al., 2018; Gu et al., 2023b). With extensive marine aquaculture, including fish, shellfish, and seaweed cultivation, the bay has experienced significant anthropogenic influences (Dong et al., 2023a; Gu et al., 2023c; Chen et al., 2024). These activities increase the organic load in sediments, altering the environmental conditions and potentially influencing the mobility, bioavailability, and stabilization of metals (Gu et al., 2014b; Gu et al., 2022a; Han et al., 2023; Gu et al., 2025a). As a representative typical marine aquaculture bay in the South China Sea, Zhelin Bay shares common environmental and anthropogenic characteristics with many coastal aquaculture areas worldwide, especially in tropical and subtropical regions. Therefore, insights gained from this study have broader implications for understanding metal cycling and ecological risks in similar coastal aquaculture ecosystems globally.

The innovation of this study lies in its detailed exploration of metal stabilization and the dynamic release behaviors in a human-impacted, aquaculture-dominated coastal bay. While previous research has focused on metal contamination and ecological risk in coastal sediments (Gu et al., 2022a; Man et al., 2022; Gu et al., 2023a; Han et al., 2023), this study is among the first to integrate Diffusive Gradients in Thin Films (DGT) technology with the DIFS model to quantitatively assess how metals are immobilized or stabilized within sediment environments influenced by aquaculture activities. By analyzing metals such as Al, Cr, Mn, Fe, Co, Ni, Cu, Zn, Cd, and Pb, this study offers a comprehensive understanding of how environmental factors—stemming from both aquaculture practices and terrestrial nutrient inputs—affect the retention, mobility, and potential ecological risks of metals in sediments. These ten metals—Al, Cr, Mn, Fe, Co, Ni, Cu, Zn, Cd, and Pb—were selected due to their ecological relevance, prevalence in aquaculture-related pollution, and distinct geochemical behaviors. For example, Fe, Mn, Cu, and Zn are redox-sensitive and influence other metal dynamics; Cd, Pb, and Cr are toxic and strictly regulated in environmental quality standards; while Al, Co, and Ni also play important roles in sediment geochemistry (Chi et al., 2021; Wang et al., 2021; Dong et al., 2023b; Gu et al., 2025b). Zhelin Bay is particularly susceptible to contamination due to its semi-enclosed hydrodynamic conditions, high-intensity aquaculture, and proximity to terrestrial nutrient inputs, all of which contribute to the accumulation and potential mobilization of these metals (Gu et al., 2023b; Chen et al., 2024; Gu et al., 2025a). Zhelin Bay is particularly susceptible to contamination due to its semi-enclosed hydrodynamic conditions, high-intensity aquaculture, and proximity to terrestrial nutrient inputs, all of which contribute to the accumulation and potential mobilization of these metals (Gu et al., 2023b; Chen et al., 2024; Gu et al., 2025a).

We hypothesize that in Zhelin Bay sediments influenced by intensive aquaculture, metal immobilization and remobilization dynamics are significantly affected by organic enrichment and redox conditions, which can be quantitatively characterized by combining DGT measurements with DIFS kinetic modeling. Specifically, we propose that the interplay between biogeochemical factors and anthropogenic inputs governs metal retention and release, influencing their ecological availability and risk profiles.

In this research, we systematically assessed the dynamics of metal release in Zhelin Bay using DGT technology with the DIFS model, offering insights into the immobilization mechanisms that govern the stability of these metals in coastal sediments. By analyzing key kinetic parameters and metal behaviors across various sites, we aimed to elucidate how metals are stabilized within the sediment matrix and assess the potential ecological risks associated with their release under changing environmental conditions.

This study provides novel insights into the kinetic mechanisms underlying metal stabilization and mobilization in marine aquaculture sediments, advancing the understanding necessary for developing targeted management strategies to mitigate metal-related ecological risks in coastal ecosystems heavily impacted by human activities.

2. Materials and methods

2.1. Study area and sample collection

The study area details can be found in Supporting Information. In July 2022, a total of twenty sites within Zhelin Bay were selected for surface sediment sampling. The sampling was conducted using a stainless-steel Peterson grab sampler (Fig. 1A). Immediately after sampling, sediment pH and salinity were assessed in situ using a multi-redox electrode system called the FJA-6 ORP depolarization method automatic measuring system, developed by Nanjing Chuan-Di Instrument & Equipment CO., LTD in China. Subsequently, the samples were carefully placed into two sealed bags using a plastic-steel spatula and stored in a foam box with ice packs to maintain their integrity during transportation. Once the samples arrived at the laboratory, they were refrigerated at a temperature of −4 °C. This refrigeration was done to facilitate the analysis of particle size, organic matter (OM), and inorganic carbonate ($CaCO_3$) present in the sediment. Additionally, a separate portion of each sample was stored at a lower temperature of −20 °C for later analysis using the Diffusive Gradients in Thin Films (DGT) technique.

2.2. Analytical methods

The detailed analytical methods for particle size, organic matter (OM), inorganic carbonate ($CaCO_3$), and metal fractions are provided in Supporting Information.

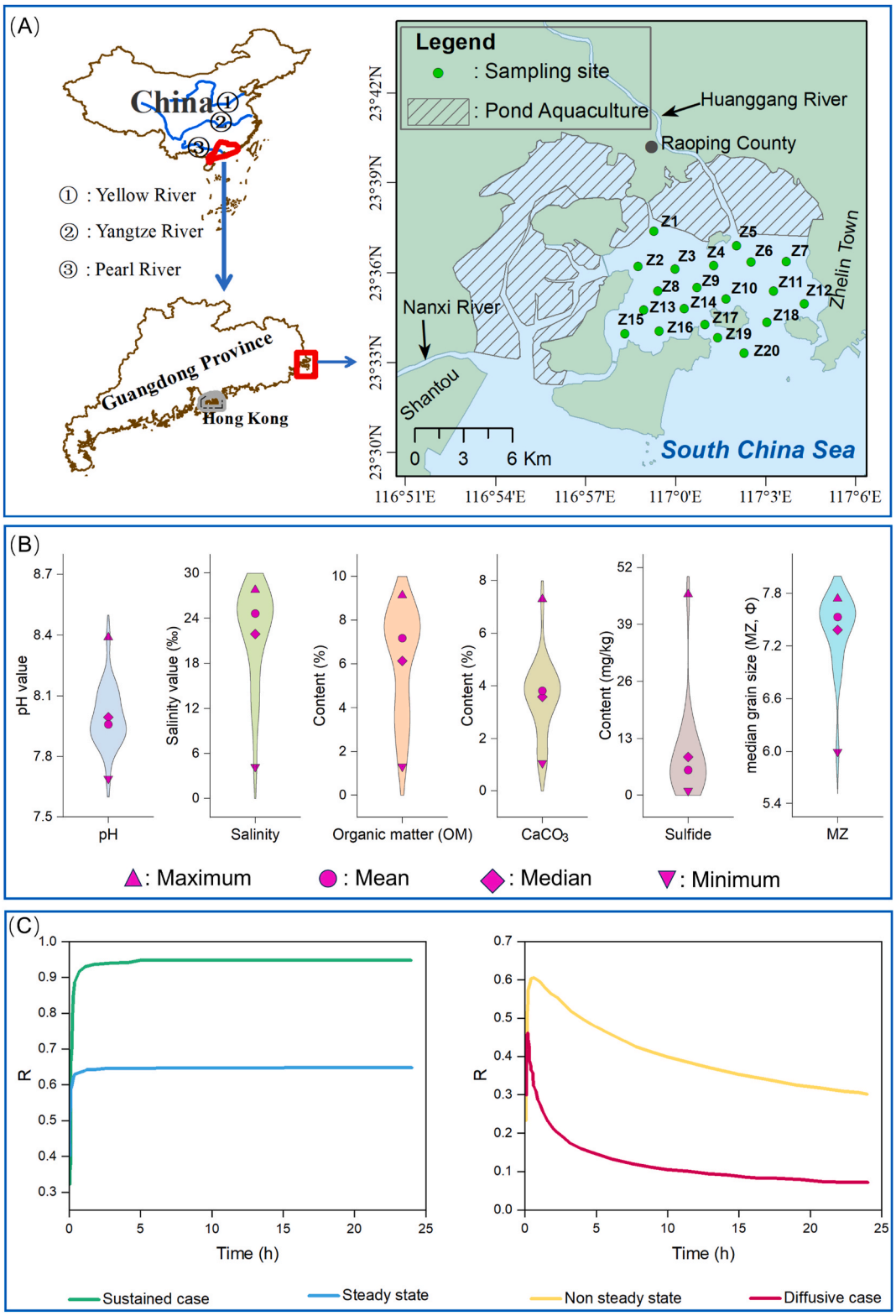

Fig. 1. (A) The study area and the sampling sites, and (B) violin plots of pH, salinity, organic matter (OM), inorganic carbonate (CaCO3), sulfide, median grain size (MZ) in surface sediments from Zhelin Bay, South China Sea; and (C) DIFS model outputs of time-dependence of the measured R values illustrating the four possible modes of resupply to the DGT devices (Harper et al., 2000; Li et al., 2021).

2.3. Quality assurance and quality control (QA/QC)

All analytical procedures followed rigorous QA/QC protocols to ensure precision and accuracy. Metal concentrations were measured using an Agilent 7700 ICP-MS equipped with a collision/reaction cell. Rhodium (Rh) and Germanium (Ge) at 5 μg/L were used as internal standards (IS) to monitor and correct for instrumental drift and matrix effects, with average IS recoveries of 99.4 % (range: 98.1 %–102.0 %).

External calibration was performed using multi-element standard solutions at 0.1, 0.5, 1, 2, 5, 10, and 20 μg/L. Calibration curves

Table 1
Input parameters used in the DIFS model and results of assumption testing.

Site	Deployment duration (s) (LSLE-NP ($Cr^{\delta+}$))	Deployment duration (s) (LSLM-NP (Al, Cd, Co, Cr^{3+}, Cu, Fe, Mn, Ni, Pb, and Zn))	Temperature (°C)	Diffusion coefficient in sediment (D_s, cm^2/s)	Diffusion coefficient in water (D_0, cm^2/s)	Diffusive layer porosity (Φ_d)	Sediment porosity (Φ_s)	△g (mm)	Particle density (P_c)	R (C_{DGT}/C_{pw})	Distribution ratio (K_d, cm^3/g)	Diffusion coefficient within the diffusive layer (D_d, cm^2/s)	Assumption and solution
Z1	87780	88260	25.13	Automatic calibration was performed by the DIFS software (2D DIFS, version 1.2.3–3, 2005, Lancaster University, UK).		0.95	Automatic calibration was performed by the DIFS software (2D DIFS, version 1.2.3–3, 2005, Lancaster University, UK).	0.92	6.64	The R value at 24 h is defined as the ratio of DGT concentration to porewater concentration. The R values for LSLE-NP at each site are provided in Table S12, while the R values for LSLM-NP at each station are listed in Tables S13–S22.	The K_d values for LSLE-NP at each site are provided in Table S12, while the K_d values for LSLM-NP at each station are listed in Tables S13–S22.	The D_d values for LSLE-NP at each site are provided in Table S12, while the K_d values for LSLM-NP at each station are listed in Tables S13–S22.	Assumption: The parameters fitted during the model solution process were T_c, k_f, and k_b, along with the variation of R values over a 24-h period. Solution: The fitted parameters include Tc, kf, and kb, as well as the variation of the R value within 24 h.
Z2	87720	88260	25.13			0.95		0.92	21.01				
Z3	87840	88260	25.13			0.95		0.92	14.22				
Z4	87900	88260	25.13			0.95		0.92	11.87				
Z5	88020	88260	25.13			0.95		0.92	16.93				
Z6	87900	88140	25.13			0.95		0.92	13.53				
Z7	87840	88020	25.13			0.95		0.92	92.62				
Z8	87840	88080	25.13			0.95		0.92	17.44				
Z9	87960	88080	25.13			0.95		0.92	12.83				
Z10	87960	88020	25.13			0.95		0.92	8.31				
Z11	88020	87780	25.13			0.95		0.92	8.63				
Z12	88020	87840	25.13			0.95		0.92	13.74				
Z13	88140	87780	25.13			0.95		0.92	7.06				
Z14	88140	87780	25.13			0.95		0.92	11.87				
Z15	88140	86520	25.13			0.95		0.92	8.57				
Z16	88080	87540	25.13			0.95		0.92	13.50				
Z17	88080	87480	25.13			0.95		0.92	15.62				
Z18	88140	87540	25.13			0.95		0.92	10.15				
Z19	88260	87600	25.13			0.95		0.92	17.91				
Z20	88320	87660	25.13			0.95		0.92	15.04				

exhibited excellent linearity ($R^2 > 0.999$), with ranges adequately covering all sample concentrations. Instrumental detection limits (DLs), calculated as three times the standard deviation (3σ) of seven replicate procedural blanks, were as follows: Al (0.420 μg/L), Cr (0.558 μg/L), Mn (0.106 μg/L), Fe (10.098 μg/L), Co (0.005 μg/L), Ni (0.071 μg/L), Cu (0.145 μg/L), Zn (0.664 μg/L), Cd (0.005 μg/L), and Pb (0.017 μg/L). Blank values were consistently below 5 % of corresponding sample concentrations and were subtracted where necessary.

To ensure data reliability, one procedural blank and one Chinese national reference material (GBW07314) were analyzed after every two environmental samples. Spiked sample recoveries ranged from 97 % to 104 %, confirming high analytical accuracy. The acid-soluble fraction (F1) extraction was validated using standard sediment sample GBW07436, with recoveries between 96 % and 105 %.

Analytical precision was assessed through triplicate measurements of selected samples, with relative standard deviations (RSDs) generally below 5 %. Accuracy and consistency were further confirmed by analyzing GBW07314 after every two test samples, with recoveries consistently between 98 % and 105 %. All materials, including labware and DGT components, were acid-cleaned and rinsed with ultrapure water (18.2 MΩ cm) prior to use.

These QA/QC protocols ensured that all metal concentration data were accurate, reproducible, and reliable throughout the analytical process.

2.4. DGT experiment and DIFS model

2.4.1. DGT experiment

The detailed procedures for the DGT experiment, including sample preparation, device deployment, and analysis, are provided in Supporting Information. The ratio (R) of C_{DGT} to C_{sed} for metals serves as an indicator of the potential ability of resupply from the solid sediment to the sediment solution. The equation can be expressed as follows:

$$R = \frac{C_{DGT}}{C_{sed}} \tag{1}$$

where C_{sed} is F1 fraction metal concentration in sediments.

2.4.2. DIFS model

The DIFS model was created to quantify these processes by employing K_d and the response time (T_c) to characterize the size of the labile pool and the kinetics of adsorption (rate constant K_f) and desorption (rate constant K_b). K_d refers to the distribution coefficient related to labile solid-phase components that can interchange with the solution phase, indicating the labile pool size within the solid phase. T_c represents the response time for depletion, which is directly linked to the supply process rate constant (K_b) from the solid phase to the solution. The model establishes a connection among R, K_d, and T_c. If R and K_d are known, T_c and kb can be determined. P_c denotes the particle concentration in the sediment, defined as $Pc = m/V$, where m signifies the total mass of solid particles, and V is the porewater volume within a specified total sediment volume. The calculation formulas are as follows (2) and (3):

$$K_d = \frac{C_{DGT}}{C_{sed}} = \frac{K_f}{P_c K_b} \tag{2}$$

$$T_c = \frac{1}{K_f + K_b} = \frac{1}{K_b(1 + K_d P_c)} \tag{3}$$

In this study, both the DGT experiment and DIFS simulation were completed at DGT® Research (www.dgtresearch.com). Metal resupply kinetics from sediments were modeled using the DIFS software (2D DIFS, version 1.2.3–3, 2005, Lancaster University, UK). The DIFS model input parameters used in this study, along with the testing of model assumptions, are summarized in Table 1. Due to space constraints, the

specific values of the parameters R, K_{dl}, and D_d are presented separately in Table S12 for LSLE-NP (Cr^{6+}) and in Table S13–S22 for LSLM-NP (Al, Cd, Co, Cr^{3+}, Cu, Fe, Mn, Ni, Pb, and Zn).

2.5. Risk assessment

2.5.1. Pollution degree models

The calculation formulas of the geoaccumulation index (I_{geo}) and enrichment factor (EF), along with their respective pollution classification criteria, are provided in the Supporting Information (Müller, 1969; Sutherland, 2000; Gu et al., 2018; Li et al., 2023a).

2.5.2. Ecological risk assessment models

To comprehensively evaluate the ecological risks posed by metals in sediments, this study employed three representative models: the Risk Assessment Code (RAC), Håkanson's Potential Ecological Risk Index (PERI), and the SPI model—an acronym derived from its three key components: Species Sensitivity Distribution (SSD), Probabilistic Risk Assessment (PRA), and the Inclusion-Exclusion Principle (IEP) (Fig. S1; Håkanson, 1980, Jain, 2004; Gu et al., 2020, Xia et al., 2025; Gu et al., 2025c). The calculation formulas and classification criteria for RAC and PERI, as well as the detailed computational procedures for the SPI model, are provided in the Supplementary Material.

2.6. Statistical analysis

Before conducting factor analysis (FA) using the principal component method, a Q-Q plot was generated for each variable to assess the normality of the dataset. According to the Q-Q plot results, all ten metal concentrations conformed to a normal distribution. Subsequently, the data were standardized using Z-scores prior to FA. All statistical analyses were performed using SPSS 19.0 for Windows.

3. Results

3.1. Sediment physicochemical properties

The values of pH, salinity, OM, $CaCO_3$, sulfide, MZ are illustrated in Fig. 1B and Table S5 in Supporting Information. The pH values were between 7.69 and 8.39 were an average of 8.00. The salinity values were in range of 4.24 ‰–27.79‰with an average of 21.93 ‰. The OM content varied from 1.33 % to 9.14 % with an average of 6.15 %, and the $CaCO_3$ content were between 1.07 % and 7.30 %, with an average of 3.59 %. The sulfide content was ranged from 1.06 mg/kg to 45.94 mg/kg with an average of 8.81 mg/kg, and the MZ values were between 6.00 Φ and 7.74 Φ with an average of 7.39 Φ.

3.2. Total and DGT-labile metal concentrations in sediments

The mean, standard deviation (SD), median, and ranges of ten metal concentrations in surface sediments of Zhelin Bay is provided in Table 2, while the spatial distributions of these metals are depicted in Fig. 2. The concentrations of the metals examined were significantly higher than their respective background values ($p < 0.01$, one-sample *t*-test), indicating strong evidence of sediment enrichment resulting from human activities (Table 2).

Generally, sites with higher metal content are found in aquaculture zones and near river estuaries (Figs. 1 and 2). The primary pathway for metals to enter the marine environment is through estuaries via rivers. The main source of anthropogenic metals in coastal marine areas comes from terrestrial origins, such as mining, metalworking, industrial processes, urban developments, and other human activities in close proximity to rivers and estuaries (Li et al., 2023a; Gu et al., 2014b; Tulcan et al., 2023). The elevated levels of metals in Zhelin Bay result from the influx of pollutants through the discharge of runoff and sewage from two rivers (Fig. 1), along with the impacts of industrialization and increasing human population (Gu et al., 2022a; Gu et al., 2023c; Han et al., 2023). Furthermore, mariculture activities, including the use of fish feeds, trash fish, and dry pellets, can also contribute to the presence of metals in the bay (Gu et al., 2014b; Han et al., 2023; Gu et al., 2017).

The average total concentrations of Cr, Cu, Zn, Cd, and Pb met Class I quality of China National Standard for marine sediments (GB18668-2002) (Table 2). Compared with other regions (Table 2), the average total metal concentrations in Zhelin Bay were comparable to those reported from those from Jiaozhou Bay (Gu et al., 2022b), intertidal zones of the Yellow River Estuary (Wang et al., 2022), Xiamen Bay (Lin et al., 2014), Rongjiang River and its estuary (Li et al., 2023a), Daya Bay (Man et al., 2022), intertidal zones of the Pearl River Estuary (Liang et al., 2023). Internationally, the metal levels also fall within the ranges reported in Weeks Bay (Paul et al., 2021), Chabahar Bay (Agah, 2021), southeastern Black Sea (Aydın et al., 2023), and Caribbean Sea (Orani et al., 2020), which represents a typical tropical marine system.

Notably, compared with the Caribbean Sea, the trace metal concentrations in Zhelin Bay are relatively lower. This contrast may reflect differences in watershed development intensity, shipping density, urban wastewater management, and sediment resuspension processes. While the Caribbean Sea receives inputs from several industrialized and densely populated coastal zones, Zhelin Bay is less urbanized and characterized by moderate aquaculture and tourism activities. These findings indicate that although Zhelin Bay shares climatic and geomorphological similarities with tropical regions like the Caribbean, the overall anthropogenic pressure is likely lower, contributing to its relatively good sediment quality and lower ecological risk.

The DGT technique has been recognized as a successful approach for acquiring information about labile metals present in sediments (Davison and Zhang, 1994; Gu et al., 2022a). In this study, the concentrations of labile metals (DGT-metals) observed at each sampling location are presented in Fig. 2. The mean (range) of the labile metals ($metal_{DGT}$) (ng/mL) were 18.37 (0.38–58.44) for Al, 0.56 (0.36–1.05) for Cr, 293.50 (3.16–2020.76) for Mn, 127.34 (42.04–264.23) for Fe, 0.37 (0.08–1.29) for Co, 3.83 (1.45–6.35) for Ni, 3.56 (2.39–4.35) for Cu, 2.39 (0.73–5.28) for Zn, 0.07 (0.02–0.15) for Cd, and 0.22 (0.05–0.48) for Pb.

The DGT technique is widely regarded as an effective *in situ* passive sampling method that simulates the bioavailability of metals to benthic organisms by measuring the labile metal fractions that are more readily absorbed biologically (Davison and Zhang, 1994; Gu et al., 2022a; Xu et al., 2024; Xia et al., 2025). Unlike total metal concentrations, DGT-labile metal levels provide a more ecologically relevant estimate of the potential exposure and toxicity to aquatic biota. Therefore, the DGT-derived data presented here serve as crucial input for subsequent probabilistic ecological risk assessments, offering a biologically meaningful basis for evaluating sediment contamination and its potential effects on marine ecosystems (Gu et al., 2022a; Gu et al., 2023a; Xu et al., 2024; Xia et al., 2025). In contrast to conventional toxicity tests using benthic organisms, which can be time-consuming and sensitive to confounding environmental variables, the DGT technique provides a rapid and reproducible method for assessing bioavailable metal(loid)s across multiple sites under natural field conditions (Gu et al., 2022a; Gu et al., 2023d; Xia et al., 2025). This makes DGT-derived data particularly suitable for probabilistic ecological risk assessments at the regional scale. In this study, the labile metal concentrations obtained by DGT were directly input into the SPI model, which integrates species sensitivity distribution (SSD), probabilistic risk assessment (PRA), and the inclusion-exclusion principle (IEP), enabling a quantitative and ecologically relevant assessment of the cumulative risks posed by multiple metals in sediments (Gu et al., 2022a; Gu et al., 2023d; Xia et al., 2025). This approach bridges field-measured bioavailability with advanced multi-pollutant risk modeling, enhancing both the accuracy and ecological relevance of sediment contamination assessments.

Table 2
Total metal concentrations in surface sediments from Zhelin Bay compared with the average total metal concentration in sediments of other regions in the world (mg/kg, dry weight).

Region	Statistical description	Al	Cr	Mn	Fe	Co	Ni	Cu	Zn	Cd	Pb
This study	Mean, SD	87291.80 ± 4880.60**	40.56 ± 7.17**	837.20 ± 234.55**	40048.14 ± 3726.79**	12.80 ± 1.39**	22.71 ± 4.20**	25.44 ± 2.52**	147.01 ± 15.01**	0.08 ± 0.01**	57.14 ± 5.19**
	Median	88053.06	40.59	834.91	40403.79	12.71	23.77	24.70	142.64	0.08	56.44
	Range	75697.362–92395.96	23.56–52.15	514.26–1361.21	32278.14–45908.76	10.27–15.61	12.64–28.82	21.58–30.28	126.84–181.75	0.06–0.12	45.37–69.49
Jiaozhou Bay, China [a]	Mean	n.a.	58.5	n.a.	n.a.	13.3	28.5	25.5	73.9	n.a.	30.1
Intertidal zones of the Yellow River Estuary, China [b]	Mean	n.a.	43.32	464.17	14,600	8.31	21.47	13.55	30.46	0.14	5.89
Xiamen Bay, China [c]	Mean	n.a.	53.5	n.a.	n.a.	n.a.	n.a.	23.4	107	0.177	40.2
Rongjiang River and its estuary, China [d]	Mean	n.a.	88.27	797.18	45,636.44	n.a.	148.25	62.08	125.18	2.38	113.40
Daya Bay, China [e]	Mean	n.a.	64.0	551.3	34,000	12.3	49.1	79.1	127.2	n.a.	50.3
Intertidal zones of the Pearl River Estuary, China [f]	Mean	n.a.	118.52	860.4	n.a.	19.47	72.55	128.13	198.5	n.a.	72.99
Weeks Bay, USA [g]	Mean	n.a.	32.0	n.a.	n.a.	6.0	n.a.	9.0	45.3	n.a.	10.5
Chabahar Bay, Iran [h]	Mean	45,000	92.3	422	31,100	13	58	14.1	39.6	2.29	9.2
Southeastern Black Sea, Turkey [i]	Mean	39,758.00	120.75	1168.53	56,659.83	17.98	44.93	82.66	155.03	0.99	93.71
Caribbean Sea [j]	Mean	46714.29 ± 25499.77	162.86 ± 185.63	69 ± 541.63	1214.29 ± 642.75	14.71 ± 13.94	67 ± 63.69	90.57 ± 57.46	202.14 ± 128.4	0.53 ± 0.26	64.29 ± 62.03
Background values [j]		73100 [k]	28.6	343	24,305	8.41	14.9	11.8	38.0	0.030	40.3
Class I upper limit [l]		n.a.	80.0	n.a.	n.a.	n.a.	n.a.	35.0	150.0	0.5	60.0
Class II upper limit [l]		n.a.	150.0	n.a.	n.a.	n.a.	n.a.	100.0	350.0	1.50	130.0
Class III upper limit [l]		n.a.	270.0	n.a.	n.a.	n.a.	n.a.	200.0	600.0	5.00	250.0

SD: standard deviation; $^{**}p < 0.01$ significant level; n.a: not available.

[a] (Gu et al., 2022b).
[b] (Wang et al., 2022).
[c] (Lin et al., 2014).
[d] (Li et al. 2023).
[e] (Man et al., 2022).
[f] (Liang et al., 2023).
[g] (Paul et al., 2021).
[h] (Agah, 2021).
[i] (Aydın et al., 2023).
[j] (Orani et al., 2020).
[k] (CEMS, 1990).
[l] The criterion of China National Standard for marine sediments (GB18668-2002). In this criterion, there are three hierarchical levels: Class I, Class II, and Class III. Each class has specific purposes and regulations. Class I represents the highest level of strictness and is primarily designated for the protection of marine habitats, including natural, rare, and endangered species, as well as areas for human recreation and sports. Class II is aimed at regulating general industrial use and coastal tourism. Class III is specifically designated for defining harbors and areas for special use related to ocean exploration.

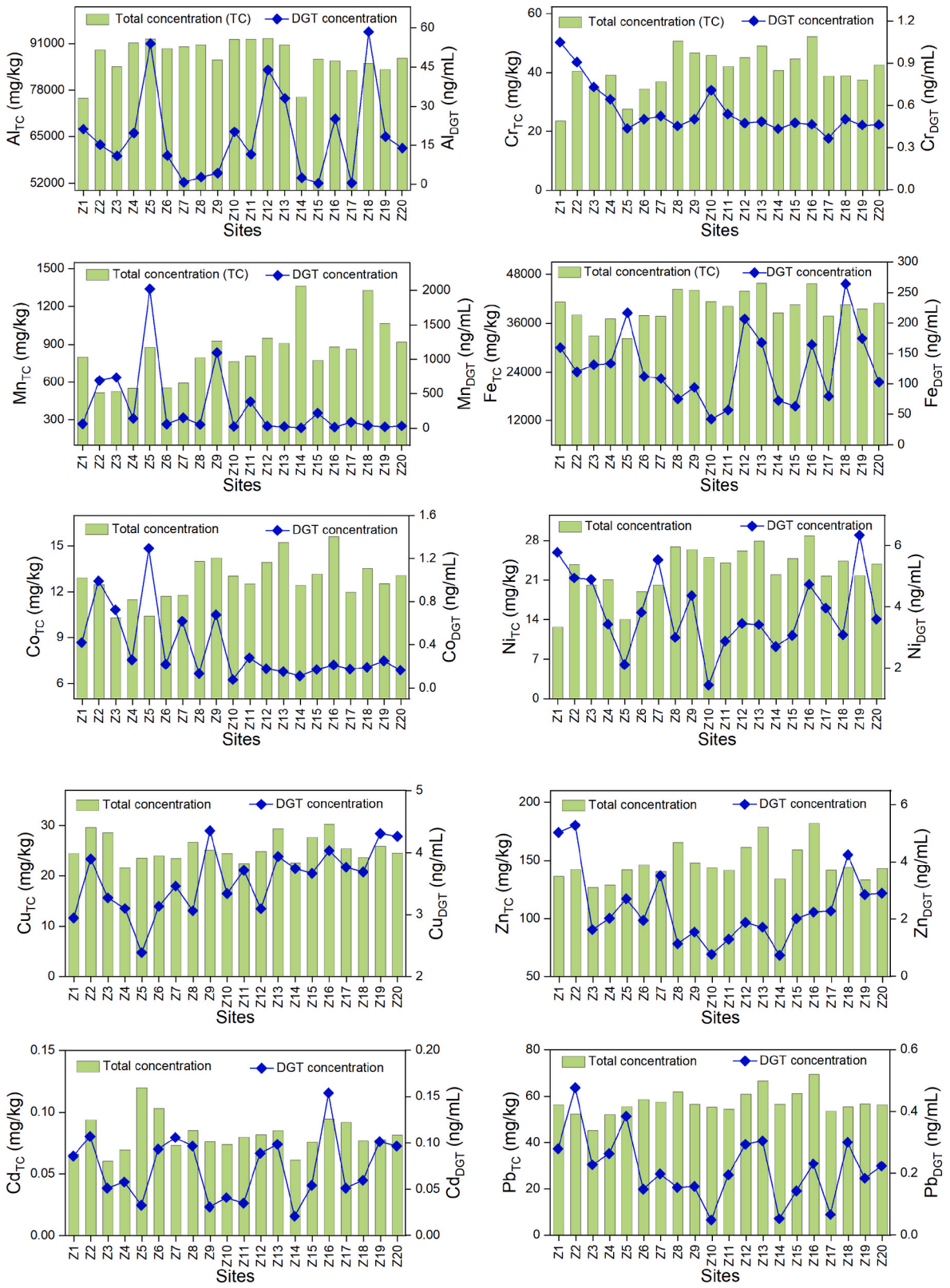

Fig. 2. Spatial distributions of total metal concentrations and DGT-labile metal concentrations in surface sediments from Zhelin Bay, South China Sea.

3.3. Release dynamic assessment by DIFS model

3.3.1. Resupply patterns of metals in sediments

The time-dependence of R values for ten metals in surface sediments across 20 sites from Zhelin Bay is presented in Fig. S2 in Supporting Information. The distribution patterns of the time-dependence of R values for pollutants can be used to determine the resupply mechanisms of metals in sediments (Harper et al., 2000; Li et al., 2021). Based on Figs. 1C and S2 in Supporting Information, we can identify the resupply modes of ten metals across the 20 sampling sites in Zhelin Bay, as shown

in Fig. 3. The resupply modes of ten metals (Al, Cr, Mn, Fe, Co, Ni, Cu, Zn, Cd, Pb) across 20 sampling sites in Zhelin Bay showed significant spatial variability. Based on DIFS model outputs, the resupply patterns of these metals were classified into four modes: Sustained Case, Steady State, Non-Steady State, and Diffusive Case (Harper et al., 2000). Overall, the metals in Zhelin Bay predominantly followed the diffusive mode, indicating limited resupply to the DGT devices.

Al predominantly followed the diffusive mode, with most sites (e.g., Z1, Z3, Z5) exhibiting diffusion-controlled resupply. Only a few locations, such as Z2 and Z12, indicated steady-state resupply, suggesting limited replenishment from sediment solids in these areas. Cr demonstrated a relatively uniform resupply pattern, with the majority of sites classified as diffusive, indicating low resupply rates relying on metal diffusion within the sediment. However, a few sites, such as Z10 and Z18, exhibited non-steady state behavior, indicating slower resupply but with noticeable depletion of the sorbed metal pool.

For Mn, there was considerable variation between sites. Some stations, such as Z6 and Z7, showed non-steady state resupply, while others were mainly governed by diffusion, suggesting localized constraints on resupply with some potential for sorbed metal replenishment. Fe followed the diffusive mode at all sites, indicating that its resupply was primarily diffusion-driven, with minimal interaction from the solid phase to replenish the porewater concentration.

Both Co and Ni exhibited diffusive resupply modes across all sampling sites, reflecting poor resupply capacity from the sediment and reliance on diffusion without significant solid-phase interaction. The resupply modes of Cu and Zn were more complex. Although most sites followed the diffusive mode, some, like Z2 and Z4, displayed steady-state resupply, suggesting a moderate capacity for resupply from the solid phase, albeit insufficient to maintain the initial porewater concentrations.

For Cd, non-steady state behavior was observed at sites such as Z3 and Z12, implying slow resupply and substantial depletion of the available sorbed metal pool, while the remaining sites predominantly exhibited a diffusive resupply mode. Pb showed diverse resupply patterns across different sites. Some stations (e.g., Z3, Z12) followed the steady-state resupply mode, while others exhibited non-steady or diffusive modes, indicating spatial heterogeneity in lead resupply potential across Zhelin Bay.

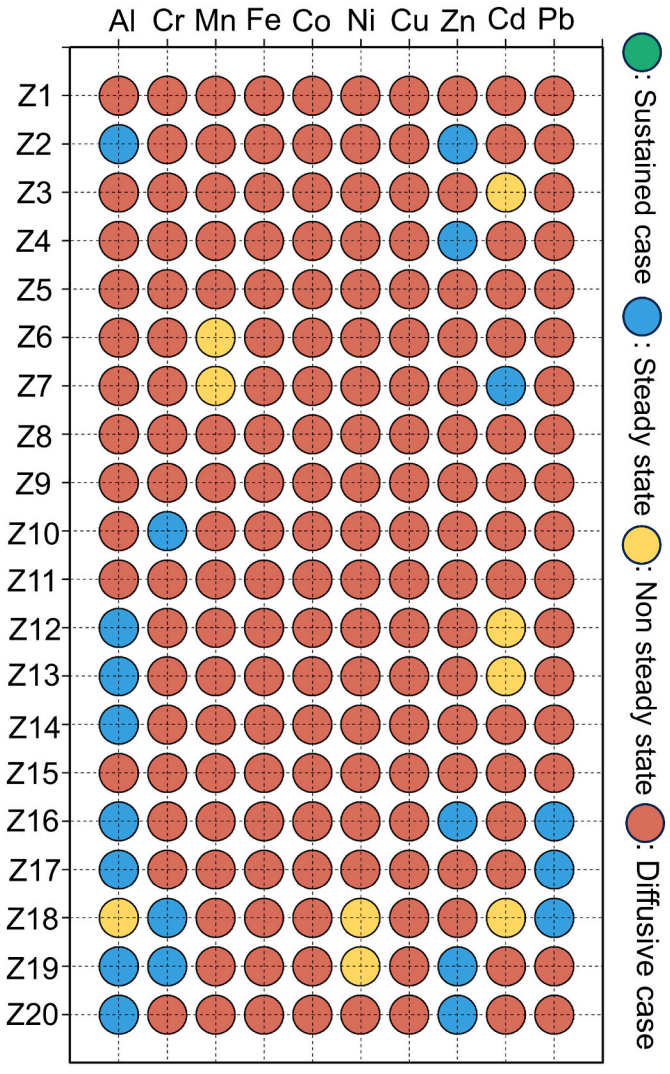

Fig. 3. Resupply modes of ten metals in surface sediments across 20 sites from Zhelin Bay, South China Sea.

3.3.2. *Labile pool size of metal (K_d)*

The K_d values and distributions for the ten metals are displayed in Table S6 in Supporting Information and Fig. S3, respectively. The K_d values indicated the metals' labile pool size in sediments, revealing their behavior and migration within the ecosystem (Gao et al., 2022; Liu et al., 2022; Chang et al., 2024). The average K_d values for the metals ranked as follows: K_d (Al) > K_d (Pb) > K_d (Zn) > K_d (Mn) > K_d (Co) > K_d (Cr) > K_d (Fe) > K_d (Cd) > K_d (Cu) > K_d (Ni) (Table S6). This trend revealed that Al exhibited the highest Kd value, indicating the strongest affinity for sediment particles, while Ni had the lowest, reflecting its weaker adsorption capacity. The variation in metal adsorption was influenced by both the inherent chemical properties of the metals and local environmental factors such as aquaculture activities, pollution inputs, and sediment characteristics.

Spatial distribution analysis revealed that K_d(Al) was particularly high around the Z15 oyster farming area, adjacent to a densely populated region in Haishan Town, suggesting a link to human activities (Fig. S3A). Elevated levels of K_d (Cr) were observed in the Z7 and Z11 regions, particularly in the estuarine zone affected by inputs from the Huanggang River, indicating upstream industrial pollution (Fig. S3B). K_d (Mn) showed significant concentrations around Z16, associated with pond farming, and also in Z6 and Z11, impacted by riverine inputs (Fig. S3C).

K_d (Fe) concentrated in the Z11 estuary, reflecting the Huanggang River's significant role in sediment contamination (Fig. S3D). K_d (Co) also showed higher activity in Z6 and Z11, with the estuarine area likely being a hotspot due to river inputs (Fig. S3E). K_d (Ni)) concentrations were greater near Z15, adjacent to populated areas, while Z6 and Z11 exhibited lower activity, suggesting stronger sediment adsorption in these locations (Fig. S3F).

K_d (Cu) displayed high activity in the Z8 seaweed farming area, indicating a potential risk to aquaculture (Fig. S3G). K_d (Zn)) had elevated levels in Z7 and Z11, suggesting industrial sources contributed to its accumulation (Fig. S3H). K_d (Cd) concentrations were high in Z11, driven by riverine pollution, and in Z16, likely due to pond farm drainage (Fig. S3I). K_d (Pb)) was elevated in Z7 and Z11, especially in oyster farming areas, reflecting the influence of land-based pollution (Fig. S3J).

In general, regions with concentrated human activities and river inputs, such as Z15, Z7, and Z11, exhibited higher levels of metal contamination.

3.3.3. *Sediment response time (T_c) of metals*

The sediment response times (T_c) for ten metals (Al, Cr, Mn, Fe, Co, Ni, Cu, Zn, Cd, and Pb) were measured at 20 sampling stations (Z1- Z20) across Zhelin Bay, as detailed in Table S7 in Supporting Information. The distributions of T_c for these metals are illustrated in Fig. S4 in Supporting Information. The T_c value represents the characteristic time required for each metal element to reach 63 % of its equilibrium concentration within the sediments (Harper et al., 2000). This parameter is essential

for understanding the kinetic behavior of metals in dynamic sedimentary environments.

General trends: The majority of metals, particularly Cr, Mn, Fe, Co, Ni, and Pb, exhibited relatively high T_c values across most stations, with the maximum T_c recorded at 10,000 s (Table S7). This indicates that these metals have slower response times, suggesting a more prolonged stabilization process in the sediment after disturbances, such as tidal movements or anthropogenic inputs. In contrast, metals like Cd and Zn displayed greater variability in their T_c values, suggesting differences in their interaction with sediment components and local environmental conditions.

Significant variations: Certain stations, notably Z5, Z12, Z13, Z16, Z17, Z18, and Z19, recorded significantly lower T_c values for metals such as Al, Cu, Cd, and Cr. For instance, at Z5, the T_c value for Al was as low as 44.5 s, indicating rapid re-equilibration. Similarly, station Z16 displayed a markedly low T_c for Pb (77.6 s), demonstrating a relatively fast sedimentary response compared to other metals at this location (Fig. S4 and Table S7).

Station-specific patterns: Distinct spatial patterns in T_c values were observed across the sampling stations. Station Z1 consistently recorded high T_c values for most metals, with exceptions in Zn (2120 s) and Cd (3810 s), indicating faster responses for these metals compared to others. Station Z12 exhibited particularly rapid response times for Al (6.3 s) and Cd (1920 s), highlighting a potential influence of localized factors such as sediment composition, organic matter content, or hydrodynamics (Fig. S4 and Table S7).

Sediment response behavior: Across all stations, Fe, Co, Mn, and Ni demonstrated uniformly high T_c values, suggesting a slower re-equilibration and potentially greater long-term retention within the sediment matrix. Conversely, metals like Al and Cd exhibited lower and more variable T_c values, indicative of a more dynamic interaction with the sediment environment. These patterns suggest that local environmental factors, including sediment texture, redox conditions, and organic content, may play significant roles in regulating the mobility and stabilization of these metals.

Ecological implications: The variation in T_c values among different metals and stations provides insight into the potential ecological risks associated with metal contamination in Zhelin Bay. Metals with prolonged T_c values, such as Cr, Fe, and Ni, may pose a longer-term threat due to their slow release from sediments, while metals with shorter T_c values, such as Cd and Al, may exhibit more rapid cycling and bioavailability under disturbed conditions. Understanding these temporal dynamics is crucial for predicting metal behavior in the sediment and their subsequent impacts on the aquatic ecosystem.

3.3.4. Adsorption-desorption behaviors of metals

The values of K_f and K_b for each metal at each site are listed in Table S8 and Table S9 in Supporting Information, respectively. The average K_f values (s^{-1}) for the ten metals were ranked as follows: Al (3.42E-02) > Mn (1.36E-02) > Ni (1.02E-02) > Zn (6.50E-03) > Pb (2.09E-03) > Cd (1.58E-03) > Cr (2.82E-04) > Cu (1.57E-04) > Co (1.23E-04) > Fe (1.16E-04) (Table S8). Similarly, the average K_b values were ordered as follows: Mn (1.38E-04) > Ni (6.64E-05) > Al (2.19E-05) > Cd (5.47E-06) > Zn (1.86E-06) > Cu (8.94E-07) > Pb (7.51E-07) > Fe (3.21E-07) > Cr (2.11E-07) > Co (1.51E-07) (Table S9).

In sediments, K_f and K_b are key parameters that describe the adsorption and release processes of metals (Gao et al., 2021; Yang et al., 2024; Ma et al., 2024). A K_f/K_b ratio greater than 1 indicates that the metals tend to adsorb, exhibiting strong adsorption capability and low release potential. The larger the ratio, the higher the stability of the metal in the sediments. Conversely, a K_f/K_b ratio less than 1 suggests that the metal tends to desorb, indicating a higher release rate and greater mobility potential. Therefore, by analyzing the magnitude of the K_f/K_b ratio, we can determine the behavioral patterns of different metals in specific sediments and their potential ecological impacts.

This study systematically analyzed the K_f and K_b parameters of metals such as Al, Cr, Mn, Fe, Co, Ni, Cu, Zn, Cd, and Pb in sediments from various sampling sites to elucidate the dynamic behaviors of each metal and their stability in sediments, as illustrated in Fig. 4. Al demonstrated significant adsorption characteristics across most sampling sites, with K_f/K_b ratios generally high. Notably, at site Z9, the ratio reached 15071.24, indicating strong stability and low release potential for Al in the sediments, suggesting a minimal risk of release (Fig. 4A). Cr also exhibited high K_f/K_b ratios at several sites, particularly at Z4, where the ratio was 607.25, reflecting its stability in the sediments (Fig. 4B). In contrast, Mn showed a much lower K_f/K_b ratio of only 13.82 at site Z5, indicating that it was easily desorbed from the sediments (Fig. 4C). This high release rate and potential for migration could have led to increased concentrations of manganese in the water, posing a threat to aquatic organisms and ecosystems. The K_f/K_b ratio for Fe was 399.54, indicating good stability, although its behavior varied across different sites (Fig. 4D).

Co exhibited a K_f/K_b ratio of 581.59 at site Z3, suggesting a moderate adsorption capacity in the sediments with relatively low release risk (Fig. 4E). Ni had a K_f/K_b ratio of 47.90 at site Z14, indicating a higher desorption capacity that could pose risks to the aquatic ecosystem in certain areas (Fig. 4F). Cu had a K_f/K_b ratio of 133.33 at site Z8, suggesting it was easily desorbed from the sediments, potentially leading to increased Cu concentrations in the water (Fig. 4G). Zn demonstrated high K_f/K_b ratios at multiple sites, reaching 1488.23 at Z2, which indicates good stability and low release potential (Fig. 4H). Cd had a K_f/K_b ratio of 245.78 at site Z6, reflecting moderate stability that necessitated further monitoring (Fig. 4I). Pb exhibited an exceptionally high K_f/K_b ratio of 18851.99 at site Z16, indicating a strong adsorption capacity in the sediments with almost no risk of release (Fig. 4J).

Generally, the comprehensive analysis of K_f/K_b ratios facilitated the assessment of metal pollution risks across different sites in Zhelin Bay. Metals with high K_f/K_b ratios, such as Al, Pb, Zn, and Cr, displayed lower ecological risks at most sites, while those with low K_f/K_b ratios, including Mn, Cu, and Ni, indicated a greater potential threat to aquatic organisms and ecosystems in specific areas. Therefore, enhanced monitoring and assessment of these metals with high desorption potential are essential to mitigate their environmental impacts.

4. Discussion

4.1. Risk assessment

The degree of metal contamination in the surface sediments of Zhelin Bay was evaluated using multiple indices. Based on total metal concentrations, the I_{geo} values (Fig. S5A) revealed that Zn levels at all sites fell between 1 and 2, indicating moderate contamination. Mn, Fe, Co, Ni, and Cu were mostly categorized as slight pollution, while Cd, Pb, and Al generally reflected an unpolluted status. EF analysis (Fig. S5B) showed that Cr, Fe, Co, Ni, Cu, and Pb were minorly enriched (EF = 1–2), implying slight anthropogenic input. In contrast, Mn, Zn, and Cd exhibited moderate enrichment (EF = 2–5), suggesting a measurable degree of human-induced contamination.

To evaluate the potential ecological risks associated with bioavailable metal fractions, RAC was applied. Al and Fe had RAC values below 1 %, indicating no ecological risk. Most other metals, including Cr, Co, Ni, Cu, Zn, Cd, and Pb, exhibited RAC values between 1 % and 10 %, denoting low risk, whereas Mn showed moderate risk (10–30 %) at most sites (Fig. S6A). The PERI, which incorporates total concentrations and toxicity coefficients, yielded Risk Index (RI) values below 188 across all sites, suggesting that sediments currently pose a low ecological risk (Fig. S6B).

However, both RAC and PERI are limited by their inability to capture combined toxic effects from multiple metals. RAC focuses solely on weak acid-exchangeable fractions without considering additive or synergistic interactions, while PERI uses empirical toxicity coefficients based on total concentrations, potentially over- or underestimating real

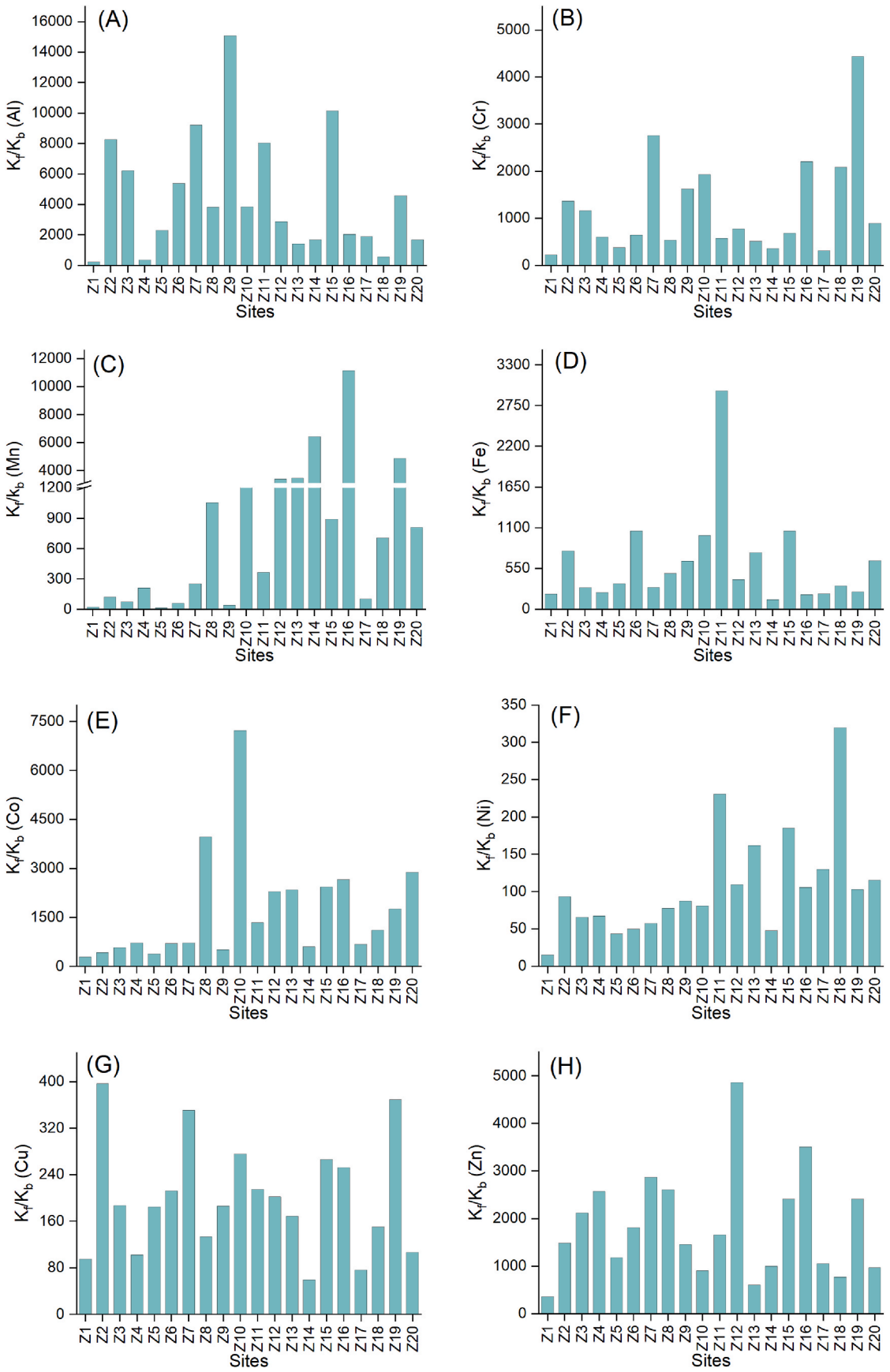

Fig. 4. Spatial distributions of K_f/K_b ratios of ten metals from Zhelin Bay, South China Sea.

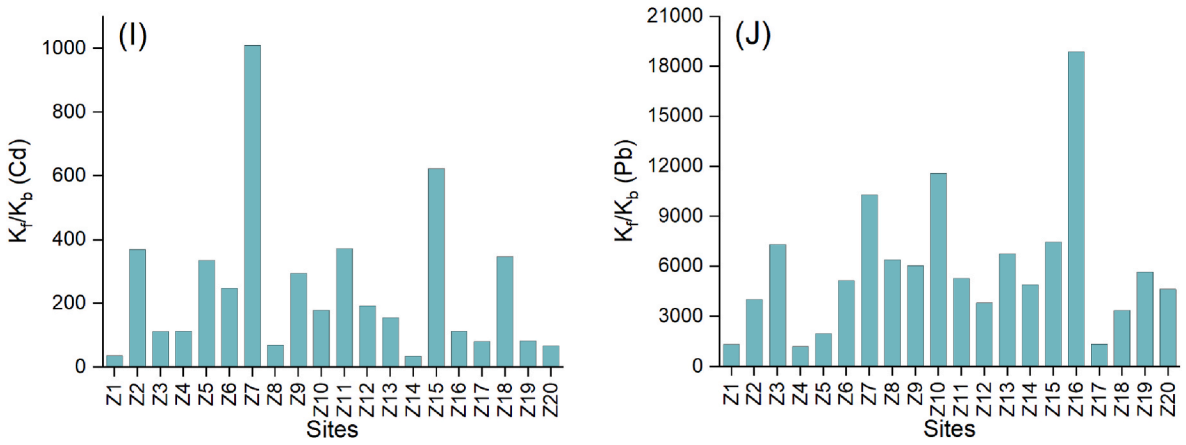

Fig. 4. (*continued*).

ecological hazards. Moreover, these indices do not account for sediment dynamic processes such as sediment reworking or bioturbation, which can alter metal bioavailability and mobility, potentially affecting ecological risks. This limitation highlights the need for models integrating dynamic sediment-metal interactions.

To overcome these limitations, we employed the SPI model (Gu et al., 2020; Gu et al., 2025c; Xia et al., 2025), which integrates bioavailable DGT-labile metal concentrations and ecotoxicological thresholds across trophic levels to estimate cumulative risk. The log-transformed DGT data followed a normal distribution (K-S test; Table S10), and probabilistic risk curves were constructed (Fig. S7). The SPI model revealed a joint ecological risk probability of 27.30 %, with Mn (11.19 %) and Al (11.15 %) being the dominant contributors (Fig. 5). These values reflect a more nuanced and ecologically realistic picture of sediment metal toxicity, emphasizing that dynamic and integrative approaches like SPI are essential to comprehensively assess the risk from co-occurring metal contaminants.

Considering the moderate joint risk and the dominant contribution of bioavailable metals, sediment management strategies should prioritize monitoring of Mn and Al species and incorporate approaches to mitigate bioavailability, thus supporting sustainable mariculture practices in Zhelin Bay. This approach aligns with international sediment management frameworks aimed at balancing environmental protection with aquaculture development.

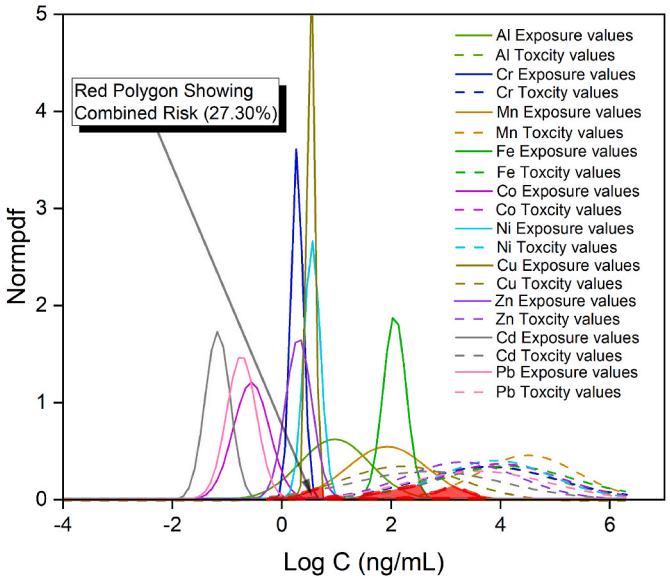

Fig. 5. Combined risk of DGT-measured metals in surface sediments from Zhelin Bay, South China Sea, assessed using the SPI model.

4.2. Metal sources

The combined application of FA and geographic information system (GIS) provides a powerful approach for identifying metal sources (Zhou et al., 2007; Gu et al., 2012). First, FA based on the principal component method is employed to reduce data dimensionality and extract key factors (Fs) along with their corresponding factor scores. Subsequently, spatial interpolation of these factor scores using GIS enables the visualization and spatial localization of potential pollution sources.

In this study, FA with VARIMAX rotation extracted three principal factors (Fs) with eigenvalues greater than 1, explaining 81.63 % of the total variance (Table S11). Prior to interpretation, the Kaiser-Meyer-Olkin (KMO) test and Bartlett's test of sphericity were conducted to assess the suitability of the dataset for FA. The KMO value was 0.63, and Bartlett's test yielded a chi-square value of 217.96 ($df = 45$, $p < 0.01$), indicating that the data were suitable for dimensionality reduction through FA.

Cr, Fe, Co, Ni, Zn, Cu, and Pb all exhibited strong positive loadings on F1, suggesting a shared anthropogenic source likely associated with industrial discharge, urban runoff, and port activities (Fig. 6A; Table S11). Spatial interpolation of F1 scores using GIS revealed that this factor was predominantly concentrated near the residential area of Haishan Town, impacting sampling sites Z8, Z9, Z10, Z12, Z13, Z15, Z16, Z18, and Z20, consistent with urban-related pollution sources (Fig. 6C and F). F2 was characterized by a high positive loading of Mn and a strong negative loading of Al (Fig. 6A; Table S11). Since Al typically represents natural geochemical background, the contrasting loadings implied that F2 primarily reflected natural geochemical processes such as sediment grain size variation, organic matter content, or redox conditions, rather than direct pollution inputs. GIS-based spatial interpolation showed that F2 scores were mainly distributed around the floating cage aquaculture zones, affecting sites Z1, Z9, Z13, Z14, Z16, Z17, Z18, Z19, and Z20, indicating the influence of aquaculture-related sediment dynamics (Fig. 6D and G). F3 was dominated solely by Cd with a high positive loading, pointing to a distinct source potentially linked to riverine inputs, agricultural runoff, or aquaculture effluents (Fig. 6B; Table S11). The spatial distribution of F3 scores was mainly concentrated within the Huanggang River estuary region, impacting sites Z1, Z2, Z5, Z6, Z8, Z12, Z13, Z16, and Z17 (Fig. 6E and H). Collectively, these results demonstrated spatially distinct origins for the metals in Zhelin Bay sediments, providing critical insights for targeted pollution control and environmental management.

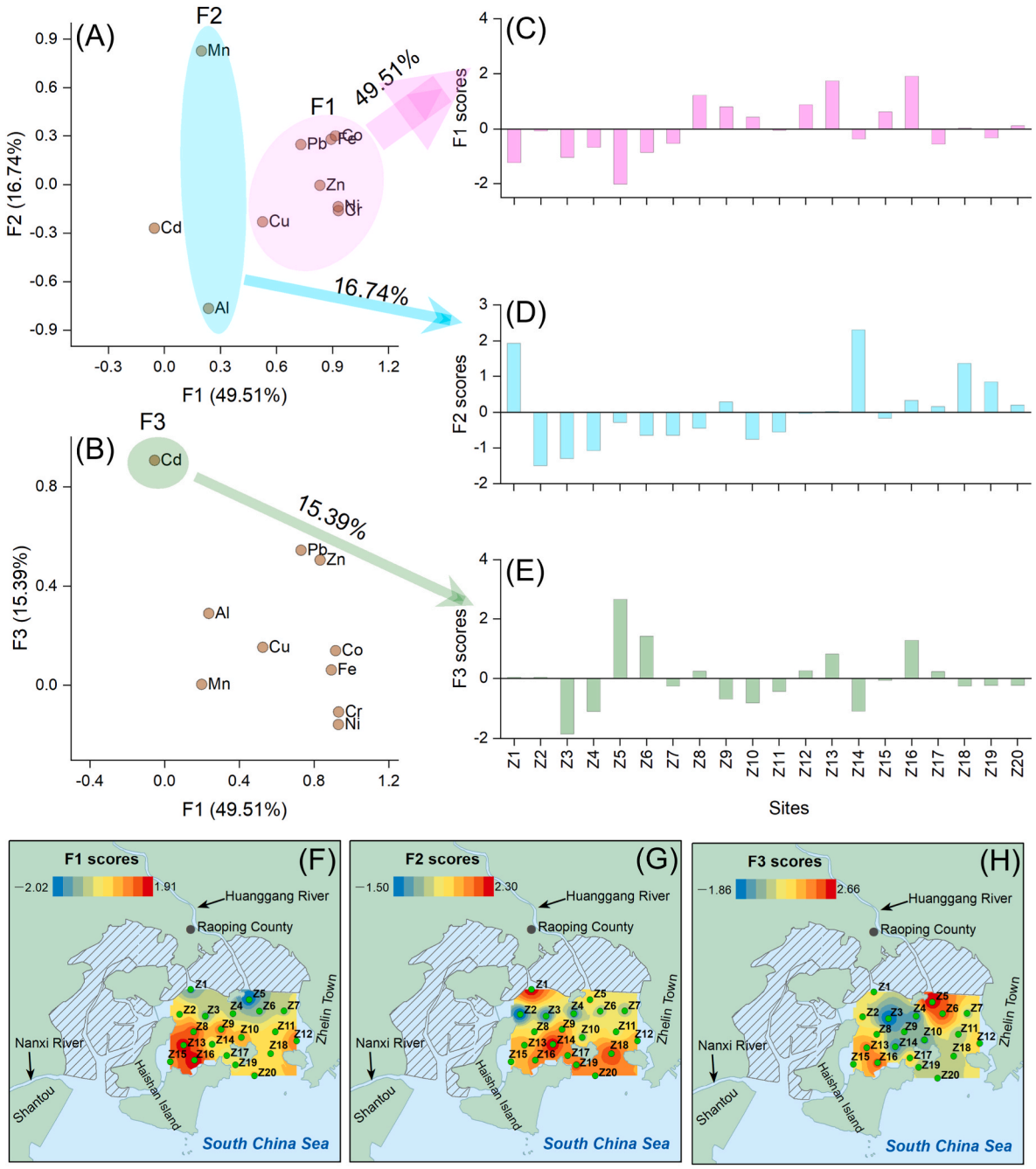

Fig. 6. Distributions of metal factor loadings (A, B), site scores (C–E), and spatial distributions of factor scores for F1 (F), F2 (G), and F3 (H) generated using the inverse distance weighting (IDW) interpolation technique in GIS.

4.3. Mechanisms of metal immobilization in sediments

In some coastal regions such as the typical marine aquaculture bay Xincun Lagoon in Hainan Province, studies have documented that over the past century, the sedimentary environment has undergone a significant transformation, transitioning from an oxidizing to a reducing environment (Gu et al., 2025b). This shift has been particularly pronounced in marine aquaculture bays, such as Zhelin Bay, due to the combined effects of natural processes and human activities. The increased input of nutrients and organic carbon from agricultural runoff, aquaculture waste, and urban development has led to widespread eutrophication, resulting in seasonal hypoxia and the accumulation of sulfides in the sediments. These environmental conditions have fostered the formation of stable metal-sulfide complexes, effectively immobilizing metals in the sediment matrix and reducing their bioavailability.

As discussed in section 3.3.1, metals such as Al, Cr, and Pb exhibited strong adsorption characteristics, with high K_f/K_b ratios, indicating that they are predominantly retained in the sediments and unlikely to desorb under current environmental conditions (section 3.3.4). This strong affinity between metals and sediment particles, particularly under reducing conditions, is a critical factor in the long-term immobilization of these metals. The data from various sampling stations in Zhelin Bay supports this observation, with many metals demonstrating extended response times (T_c), as highlighted in section 3.3.3, further suggesting that they are slow to reach equilibrium with overlying water, remaining immobilized in the sediments.

The formation of sulfide-metal complexes is a well-documented

mechanism that contributes to this immobilization. Metals such as Cd, Zn, and Pb readily form stable precipitates with sulfides in reducing environments, significantly lowering their mobility. This process was particularly evident at several stations where sulfide-rich sediments correlated with lower K_f values for these metals, as noted in section 3.3.2. For example, Pb exhibited exceptionally low desorption potential across most sites (section 3.3.4), aligning with the hypothesis that it is effectively sequestered in the form of metal-sulfide complexes. In addition, local variations in sediment composition, organic matter content, and redox conditions may play a role in modulating the stability of these metals in specific areas.

Nevertheless, alternative processes such as sediment reworking and bioturbation—common in marine aquaculture environments—can disrupt these immobilization mechanisms by physically mixing sediments and altering redox gradients. Such activities may enhance metal remobilization and bioavailability, a factor not directly captured in the present study but important for understanding temporal and spatial variability in metal behavior. Future investigations integrating bioturbation effects and sediment dynamics are needed to fully elucidate these processes, as recognized in recent international sediment research (e.g., Arlinghaus et al., 2021; Cozzoli et al., 2021; Pan et al., 2023).

The ecological implications of metal immobilization in sediments are significant. While metals that remain immobilized in the sediment pose a reduced immediate risk to aquatic organisms, any environmental disturbance—such as dredging, storms, or changes in redox conditions—could potentially remobilize these metals, leading to increased bioavailability and subsequent toxicity. Therefore, understanding the conditions that promote or disrupt this immobilization mechanism is crucial for managing the ecological health of aquaculture bays like Zhelin Bay.

In general, the transition to a reducing environment, combined with increased organic input and subsequent sulfide formation, has created conditions that favor the long-term immobilization of certain metals in the sediments of Zhelin Bay. This immobilization process is highly dependent on the specific metal and local environmental conditions, with some metals showing greater susceptibility to remobilization than others. This complexity underscores the need for sediment management strategies that consider not only chemical speciation but also physical and biological sediment processes to safeguard aquaculture sustainability. Continued monitoring and further research into the stability of these metal-sediment interactions under varying environmental conditions will be essential for predicting future ecological risks.

4.4. Limitations of the study

This study offers valuable insights into the mechanisms of metal immobilization and the associated ecological risks in coastal mariculture sediments. Nonetheless, several limitations merit explicit acknowledgment to contextualize the findings. The research is constrained by a single-season sampling campaign conducted solely in July, thereby limiting the temporal representativeness and precluding assessment of seasonal or interannual variability in sediment characteristics and metal dynamics. The ecological risk assessment predominantly relies on probabilistic modeling of bioavailable metal concentrations, exemplified by the SPI model, which integrates ecotoxicological thresholds across multiple trophic levels. However, the absence of direct biological endpoints or in situ bioassays limits empirical validation of the predicted toxicological impacts on aquatic organisms. Furthermore, the analytical framework assumes sediment processes are close to equilibrium, potentially underestimating the influence of dynamic natural disturbances—such as bioturbation, sediment reworking, storm events—and anthropogenic activities, all of which can significantly affect metal mobility and bioavailability. To enhance the robustness and ecological relevance of future research, it is recommended to incorporate multi-seasonal sampling schemes, integrate direct biological effect assessments, and develop dynamic modeling approaches that explicitly account for environmental disturbances.

5. Conclusion

This study systematically investigated the release dynamics of ten metals (Al, Cr, Mn, Fe, Co, Ni, Cu, Zn, Cd, and Pb) in the sediments of Zhelin Bay using DGT technology and the DIFS model. All metals showed a general trend toward adsorption and stabilization, indicating limited short-term mobility under current environmental conditions. Sediment biogeochemistry, influenced by aquaculture activities and terrestrial nutrient inputs, played a key role in metal behavior. To evaluate potential ecological risks, a probabilistic assessment based on the SPI model was applied. This approach integrates experimentally derived toxicity data from aquatic biota across different trophic levels with a statistical framework to estimate cumulative risk. However, the assessment is predictive in nature and does not include direct in situ biological measurements. Therefore, conclusions regarding ecological safety should be interpreted with caution. Further research combining geochemical analyses with biological investigations is needed to fully understand the ecological implications of metal dynamics in aquaculture-impacted coastal systems.

CRediT authorship contribution statement

Yang-Guang Gu: Writing – review & editing, Visualization, Supervision, Resources, Methodology, Funding acquisition, Data curation, Writing – original draft, Validation, Software, Project administration, Investigation, Formal analysis, Conceptualization. **Yanpeng Gao:** Investigation, Validation, Funding acquisition. **Richard W. Jordan:** Writing – review & editing. **Shi-Jun Jiang:** Writing – review & editing.

Environmental implication

The findings of this study hold significant environmental implications, particularly for coastal ecosystems affected by aquaculture and nutrient runoff. By demonstrating how metals become immobilized in sediments through strong adsorption and stable metal-sulfide complex formation, we revealed the potential for reduced mobility and ecological risk under current conditions. However, the susceptibility of these metals to remobilization during environmental disturbances underscores the need for ongoing monitoring. Understanding these dynamics is crucial for effective management strategies aimed at preserving aquatic health and mitigating the long-term impacts of anthropogenic activities on sediment biogeochemistry in marine environments.

Declaration of competing interest

The authors declare that they have no known competing financial interests or personal relationships that could have appeared to influence the work reported in this paper.

Acknowledgments

This study was supported by the National Key R&D Program of China (2022YFC3105600, 2024YFD2401401), National Natural Science Foundation of China (42322704, 42277222), Guangdong Basic and Applied Basic Research Foundation (2023B1515020078) and Central Public-interest Scientific Institution Basal Research Fund, CAFS (2023TD15).

Appendix A. Supplementary data

Supplementary data to this article can be found online at https://doi.org/10.1016/j.envpol.2025.126798.

Data availability

Data will be made available on request.

References

Agah, H., 2021. Ecological risk assessment of heavy metals in sediment, fish, and human hair from Chabahar Bay, Makoran, Iran. Mar. Pollut. Bull. 169, 112345.

Arlinghaus, P., Zhang, W., Wrede, A., Schrum, C., Neumann, A., 2021. Impact of benthos on morphodynamics from a modeling perspective. Earth Sci. Rev. 221, 103803.

Aydın, H., Tepe, Y., Ustaoğlu, F., 2023. A holistic approach to the eco-geochemical risk assessment of trace elements in the estuarine sediments of the Southeastern Black Sea. Mar. Pollut. Bull. 189, 114732.

CEMS (China Environmental Monitoring Station), 1990. China Environmental Science Press 22–33.

Chang, X., Duan, T.T., Feng, J.S., Li, Y.X., 2024. Contrasting fate and binding behavior of Mn and Cu with dissolved organic matter during in situ remediation using multicomponent capping in malodorous black water. Water Res. 253, 121288.

Chen, Z.P., Luo, F., Zhu, F., Wu, H.B., Li, R.J., Tao, A.F., 2024. Impact of engineering measures on water exchange and water quality in semi-closed bay: a model study in Zhelin Bay. Regional Studies in Marine Science 77, 103722.

Chi, G.X., Liu, B.L., Hu, K., Yang, J., He, B.C., 2021. Geochemical composition of sediments in the Liao River Estuary and implications for provenance and weathering. Regional Studies in Marine Science 45, 101833.

Cozzoli, F., Shokri, M., Gomes da Conceição, T., Herman, P.M.J., Hu, Z., Soissons, L.M., Van Dalen, J., Ysebaert, T., Bouma, T.J., 2021. Modelling spatial and temporal patterns in bioturbator effects on sediment resuspension: a biophysical metabolic approach. Sci. Total Environ. 792, 148215.

Davison, W., Zhang, H., 1994. *In situ* speciation measurements of trace components in natural waters using thin-film gels. Nature 367 (6463), 546–548.

Dong, D., Huang, H.M., Gao, Q., Chen, M.R., Yang, X., 2023a. Conservation gap analysis of coastal blue carbon ecosystems: taking Guangdong and Guangxi as examples. Journal of Marine Sciences 41 (1), 110–120.

Dong, H.L., Zeng, Q., Sheng, Y.Z., Chen, C.M., Yu, G.H., Kappler, A., 2023b. Coupled iron cycling and organic matter transformation across redox interfaces. Nat. Rev. Earth Environ. 4 (9), 659–673.

Falkowski, P.G., Fenchel, T., Delong, E.F., 2008. The microbial engines that drive earth's biogeochemical cycles. Science 320 (5879), 1034–1039.

Gao, L., Sun, K., Xu, D.Y., Zhang, K.L., Gao, B., 2022. Equilibrium partitioning behaviors and remobilization of trace metals in the sediment profiles in the tributaries of the three gorges reservoir, China. Sci. Total Environ. 849, 157882.

Gao, L., Li, R., Liang, Z.B., Hou, L., Chen, J.Y., 2021. Seasonal variations of cadmium (Cd) speciation and mobility in sediments from the Xizhi River basin, South China, based on passive sampling techniques and a thermodynamic chemical equilibrium model. Water Res. 207, 117751.

Gu, Y.G., Wang, Z.H., Lu, S.H., Jiang, S.J., Mu, D.H., Shu, Y.H., 2012. Multivariate statistical and GIS-based approach to identify source of anthropogenic impacts on metallic elements in sediments from the mid Guangdong coasts, China. Environ. Pollut. 163, 248–255.

Gu, Y.G., Yang, Y.F., Lin, Q., 2014a. Acid volatile sulfide and simultaneously extracted metals in sediments of Nan'ao Isaland, a mariculture base in Guangdong coast, China. Journal of Shenzhen University Science and Engineering 31 (2), 198–204.

Gu, Y.G., Lin, Q., Jiang, S.J., Wang, Z.H., 2014b. Metal pollution status in Zhelin Bay surface sediments inferred from a sequential extraction technique, South China Sea. Mar. Pollut. Bull. 81 (1), 256–261.

Gu, Y.G., Ouyang, J., Ning, J.J., Wang, Z.H., 2017. Distribution and sources of organic carbon, nitrogen and their isotopes in surface sediments from the largest mariculture zone of the eastern Guangdong coast, South China. Mar. Pollut. Bull. 120 (1–2), 286–291.

Gu, Y.G., Ke, C.L., Liu, Q., 2018. Characterization, sources, and ecological hazards of polycyclic aromatic hydrocarbons in the intertidal sediments of Zhelin Bay, the biggest mariculture area on the eastern Guangdong coast of China. Mar. Pollut. Bull. 130, 192–197.

Gu, Y.G., Gao, Y.P., Huang, H.H., Wu, F.X., 2020. First attempt to assess ecotoxicological risk of fifteen rare earth elements and their mixtures in sediments with diffusive gradients in thin films. Water Res. 185, 116254.

Gu, Y.G., Gao, Y.P., Chen, F., Huang, H.H., Yu, S.H., Jordan, R.W., Jiang, S.J., 2022a. Risk assessment of heavy metal and pesticide mixtures in aquatic biota using the DGT technique in sediments. Water Res. 224, 119108.

Gu, X., Wang, Z.X., Wang, J., Ouyang, W., Wang, B.D., Xin, M., Lian, M.S., Lu, S., Lin, C. Y., He, M.C., Liu, X.T., 2022b. Sources, trophodynamics, contamination and risk assessment of toxic metals in a coastal ecosystem by using a receptor model and Monte Carlo simulation. J. Hazard Mater. 424, 127482.

Gu, Y.G., Wang, Y.S., Jordan, R.W., Su, H., Jiang, S.J., 2023a. Probabilistic ecotoxicological risk assessment of heavy metal and rare earth element mixtures in aquatic biota using the DGT technique in coastal sediments. Chemosphere 329, 138592.

Gu, Y.G., Wang, X.N., Wang, Z.H., Jordan, R.W., Jiang, S.J., 2023b. Rare earth elements in sediments from a representative Chinese mariculture bay: characterization, DGT-based bioaccessibility, and probabilistic ecological risk. Environ. Pollut. 335, 122338.

Gu, Y.G., Gao, Y.P., Jiang, S.J., Jordan, R.W., Yang, Y.F., 2023c. Ecotoxicological risk of antibiotics and their mixtures to aquatic biota with the DGT technique in sediments. Ecotoxicology 32 (4), 536–543.

Gu, Y.G., Gao, Y.P., Jordan, R.W., Jiang, S.J., Huang, H.H., 2025c. Rising temperatures lower rare earth element bioavailability and ecological risks in coastal sediments. Environ. Chem. Lett. https://doi.org/10.1007/s10311-025-01864-1.

Gu, Y.G., Jiang, S.J., Jordan, R.W., Huang, H.H., Wu, F.X., 2023d. Nonmetric multidimensional scaling and probabilistic ecological risk assessment of trace metals in surface sediments of Daya Bay (China) using diffusive gradients in thin films. Sci. Total Environ. 867, 161433.

Gu, Y.G., Wang, Y.S., Jordan, R.W., Gao, Y.P., Huang, H.H., Jiang, S.J., 2025a. Impact of coastal industrialization and urbanization on marine phosphorus cycle: insights from Daya Bay and Zhelin Bay. Gondwana Res. 140, 81–88.

Gu, Y.G., Li, H.S., Su, H., Jordan, R.W., Liang, R.Z., Jiang, S.J., 2025b. Coastal redox shifts over the past 167 years and preservation of total organic carbon and total nitrogen. Mar. Pollut. Bull. 212, 117519.

Han, Y.J., Liang, R.Z., Li, H.S., Gu, Y.G., Jiang, S.J., Man, X.T., 2023. Distribution, multi-index assessment, and sources of heavy metals in surface sediments of Zhelin Bay, a typical mariculture area in southern China. Toxics 11 (2), 150.

Harper, M.P., Davison, W., Tych, W., 2000. DIFS—A modelling and simulation tool for DGT induced trace metal remobilisation in sediments and soils. Environ. Model. Software 15 (1), 55–66.

Håkanson, L., 1980. An ecological risk index for aquatic pollution control. A sedimentological approach. Water Res. 14, 975–1001.

Jain, C.K., 2004. Metal fractionation study on bed sediments of River Yamuna, India. Water Res. 38, 569–578.

Jiskra, M., Heimbürger-Boavida, L.-E., Desgranges, M.-M., Petrova, M.V., Dufour, A., Ferreira-Araujo, B., Masbou, J., Chmeleff, J., Thyssen, M., Point, D., Sonke, J.E., 2021. Mercury stable isotopes constrain atmospheric sources to the ocean. Nature 597 (7878), 678–682.

Kumar Chaudhary, D., Bajagain, R., Seo, D., Hong, Y., Han, S., 2023. Depth-dependent microbial communities potentially mediating mercury methylation and various geochemical processes in anthropogenically affected sediments. Environ. Res. 237, 116888.

Li, H.S., Gu, Y.G., Liang, R.Z., Wang, Y.S., Jordan, R.W., Wang, L.G., Jiang, S.J., 2023a. Heavy metals in riverine/estuarine sediments from an aquaculture wetland in metropolitan areas, China: characterization, bioavailability and probabilistic ecological risk. Environ. Pollut. 324, 121370.

Li, Y.Y., Han, C., Luo, J., Jones, K.C., Zhang, H., 2021. Use of the dynamic technique DGT to determine the labile pool size and kinetic resupply of pesticides in soils and sediments. Environ. Sci. Technol. 55 (14), 9591–9600.

Li, Z., Li, X.Z., Wang, S.H., Che, F.F., Zhang, Y., Yang, P.J., Zhang, J.B., Liu, Y.X., Guo, H. C., Fu, Z.H., 2023b. Adsorption and desorption of heavy metals at water sediment interface based on bayesian model. J. Environ. Manag. 329, 117035.

Liang, R.Z., Gu, Y.G., Li, H.S., Han, Y.J., Niu, J., Su, H., Jordan, R.W., Man, X.T., Jiang, S. J., 2023. Multi-index assessment of heavy metal contamination in surface sediments of the Pearl River estuary intertidal zone. Mar. Pollut. Bull. 186, 114445.

Lin, C., Liu, Y., Li, W.Q., Sun, X.W., Ji, W.D., 2014. Speciation, distribution, and potential ecological risk assessment of heavy metals in Xiamen Bay surface sediment. Acta Oceanol. Sin. 33 (4), 13–21.

Lin, B., Pan, F., 2023. Applications of DGT in coastal sediments: monitoring and biogeochemical study of trace metals and oxyanions. Trends in Environmental Analytical Chemistry 39, e00207.

Liu, W.J., Hu, T.P., Mao, Y., Shi, M.M., Cheng, C., Zhang, J.Q., Qi, S.H., Chen, W., Xing, X.L., 2022. The mechanistic investigation of geochemical fractionation, bioavailability and release kinetic of heavy metals in contaminated soil of a typical copper-smelter. Environ. Pollut. 306, 119391.

Liu, Q.X., Jia, Z.Z., Liu, G.Z., Li, S.Y., Hu, J.T., 2023. Assessment of heavy metals remobilization and release risks at the sediment-water interface in estuarine environment. Mar. Pollut. Bull. 187, 114517.

Long, L., Liu, H., Cui, M.C., Zhang, C.L., Liu, C., 2024. Offshore aquaculture in China. Rev. Aquacult. 16 (1), 254–270.

Luo, M.Y., Zhou, C.Y., Ma, T.H., Guo, W., Percival, L., Baeyens, W., Gao, Y., 2022. Anthropogenic activities influence the mobilization of trace metals and oxyanions in coastal sediment porewaters. Sci. Total Environ. 839, 156353.

Ma, T.H., Perrot, V., Baeyens, W., Li, G., Lievens, S., Ngo, H.T.T., Nguyen, T.T.T., Leermakers, M., Gao, Y., 2024. Mercury distribution, mobilization and bioavailability in polluted sediments of Scheldt Estuary and Belgian coastal zone. J. Hazard Mater. 465, 133209.

Man, X.T., Huang, H.H., Chen, F., Gu, Y.G., Liang, R.Z., Wang, B.G., Jordan, R.W., Jiang, S.J., 2022. Anthropogenic impacts on the temporal variation of heavy metals in Daya Bay (South China). Mar. Pollut. Bull. 185, 114209.

Miranda, L.S., Wijesiri, B., Ayoko, G.A., Egodawatta, P., Goonetilleke, A., 2021. Water-sediment interactions and mobility of heavy metals in aquatic environments. Water Res. 202, 117386.

Müller, G., 1969. Index of geoaccumulation in sediments of the Rhine River. Geojournal 2 (3), 108–118.

Norgbey, E., Li, Y.P., Zhu, Y., Nwankwegu, A.S., Bofah-Buah, R., Nuamah, L., Pu, Y.S., 2021. Combined use of high-resolution dialysis, diffusive gradient in thin films (DGT) technique, and conventional methods to assess trace metals in reservoir sediments. Environ. Monit. Assess. 193, 469.

Orani, A.M., Vassileva, E., Azemard, S., Alonso-Hernandez, C., 2020. Trace elements contamination assessment in marine sediments from different regions of the Caribbean Sea. J. Hazard Mater. 399, 122934.

Pan, F., Xiao, K., Cai, Y., Li, H.L., Guo, Z.R., Wang, X.H., Zheng, Y., Zheng, C.M., Bostick, B.C., Michael, H.A., 2023. Integrated effects of bioturbation, warming and sea-level rise on mobility of sulfide and metalloids in sediment porewater of mangrove wetlands. Water Res. 233, 119788.

Paul, V., Sankar, M.S., Vattikuti, S., Dash, P., Arslan, Z., 2021. Pollution assessment and land use land cover influence on trace metal distribution in sediments from five aquatic systems in southern USA. Chemosphere 263, 128243.

PRC State Council (The State Council of the People's Republic of China), 2024. Guangdong accelerates the development of a fully integrated modern marine ranching System. https://www.gov.cn/lianbo/difang/202408/content_6969599.htm.

Ray, N.E., Bonaglia, S., Cavan, E.L., Sampaio, F.G., Gephart, J.A., Hillman, J.R., Hornborg, S., Paradis, S., Petrik, C.M., Tiano, J., Yuan, J., 2025. Biogeochemical consequences of marine fisheries and aquaculture. Nat. Rev. Earth Environ. 6, 163–177.

Sun, Q., Burton, E.D., Si, D.F., Fan, T.T., Cheng, H., Yu, Z.H., Shao, X.H., Cui, P.X., Wang, Y.J., 2023. Coupling of dissolved organic matter molecular fractionation with iron and sulfur transformations during sulfidation–reoxidation cycling. Environ. Sci. Technol. 57 (43), 16327–16339.

Sutherland, R.A., 2000. Bed sediment-associated trace metals in an urban stream, Oahu, Hawaii. Environ. Geol. 39, 611–627.

Tulcan, R.X.S., Ouyang, W., Guo, Z.W., Lin, C.Y., Gu, X., Wang, A.H., Wang, B.D., 2023. Watershed seasonality regulating vanadium concentrations and ecological risks in the coastal aquatic habitats of the northwest Pacific. Environ. Pollut. 322, 121145.

Wang, X.N., Cui, L., Li, J., Zhang, C., Gao, X.Y., Fan, B., Liu, Z.T., 2021. Water quality criteria for the protection of human health of 15 toxic metals and their human risk in surface water, China. Environ. Pollut. 276, 116628.

Wang, Z., Lin, K.X., Liu, X.S., 2022. Distribution and pollution risk assessment of heavy metals in the surface sediment of the intertidal zones of the Yellow River Estuary, China. Mar. Pollut. Bull. 174, 113286.

Wang, Q., Sun, X., Lin, S.J., Dong, Y.H., Shen, H.T., He, Z.L., Luo, H.T., Zou, L.G., Chung, I.K., Yang, Y.F., 2025. Large-scale seaweed cultivation as a nature solution for carbon-negative economy and restorative environmental stewardship: lessons from China. Renew. Sustain. Energy Rev. 207, 114954.

Xia, W., Zhang, T.X., Li, X., Gao, Y.P., Jordan, R.W., Su, H., Jiang, S.J., Gu, Y.G., 2025. Nutrients and metal(loid)s in surface sediments of the Chishui River: a DGT-based assessment of the last natural tributary of the upper Yangtze River (China). Environ. Res. 275, 121455.

Xu, D.J., Xiong, H.Y., Wu, Q.L., Xiao, W.Z., Simpson, S.L., Tan, Q.G., Chen, R., Xie, M.W., 2024. Sediment ballet: unveiling the dynamics of metal bioavailability in sediments following resuspension and reequilibration. Environ. Sci. Technol. 58, 22755–22765.

Yang, D.X., Fang, W., Zhang, H., Gu, X.Y., Chen, H.Y., Sun, H.T., Luo, J., 2024. Migration and availability of Ni and Cd in industrial soils under different leaching conditions: insights from DGT and DIFS models. J. Hazard Mater. 480, 135863.

Zhou, F., Guo, H.C., Hao, Z.J., 2007. Spatial distribution of heavy metals in Hong Kong's marine sediments and their human impacts: a GIS-based chemometric approach. Mar. Pollut. Bull. 54, 1372–1384.

Zitoun, R., Marcinek, S., Hatje, V., Sander, S.G., Völker, C., Sarin, M., Omanović, D., 2024. Climate change driven effects on transport, fate and biogeochemistry of trace element contaminants in coastal marine ecosystems. Commun. Earth Environ. 5 (1), 560.